T03

hep-ex/0107027

Study of e^+e^- Collisions in the 1.5–3 GEV C.M. Energy Region Using ISR at BABAR

E.P. Solodov
Budker Institute of Nuclear Physics, Novosibirsk
for the Collaboration

A preliminary analysis of low-energy e^+e^- collision data produced via initial state radiation (ISR) has been performed using $22\,fb^{-1}$ of BABAR data. The selection of data samples corresponding to the $\mu^+\mu^-$, $\pi^+\pi^-$, K^+K^-, $p\bar{p}$, $K^+K^-\pi^0$, 3π, 4π, 5π, 6π, 7π final states accompanied by the emitted ISR hard photon has been demonstrated. The invariant mass of the hadronic final state defines the effective collision c.m. energy, and so BABAR ISR data can be compared to the relevant direct e^+e^- measurements. The resulting distributions are already competitive with DCI and ADONE data in the 1.4–3.0 GeV energy range. In particular, they do not suffer from the relative normalization uncertainties observed for certain reactions when results from different experiments are combined. Eventually, such data may be used to measure the energy dependence of R, the ratio of the $e^+e^- \to hadrons$ and $e^+e^- \to \mu^+\mu^-$ cross sections, in the low-energy regime where precise measurements will have an impact on the interpretation of the new $(g-2)_\mu$ measurements.

1. INTRODUCTION

The possibility of using the initial state radiation (ISR) of hard photons at B-factories to study hadronic final state production in e^+e^- collisions at lower c.m. energies has been discussed previously [1, 2]. Preliminary studies of some particular ISR processes have been performed with BABAR data [3, 4]. This paper reports preliminary results from a relatively simple pilot analysis of exclusive hadronic final states accompanied by a hard (1–9 GeV) photon assumed to result from ISR. Events corresponding to $e^+e^- \to \mu^+\mu^-\gamma$ are selected also, since these enable the normalization of the hadronic cross section measurements. ISR photons are produced at all angles relative to the collision axis, and it has been shown [1] that the BABAR acceptance for such photons is around 10–15%. The analysis samples are selected from $22\,fb^{-1}$ of BABAR $\Upsilon(4S)$ and continuum data collected in 1999–2000.

The ISR cross section for a particular final state f, with e^+e^- cross section $\sigma_f(s)$, is obtained, to first order, from:

$$\frac{d\sigma(s,x)}{dx} = W(s,x)\cdot\sigma_f(s(1-x)),$$

where $x = (2E_\gamma)/\sqrt{s}$; E_γ is the energy of the ISR photon in the nominal c.m. frame, and $\sqrt{s}$ is the nominal c.m. energy. The function

$$W(s,x) = \beta\cdot((1+\delta)\cdot x^{(\beta-1)} - 1 + \frac{x}{2})$$

describes the energy spectrum of the ISR photons;

$$\beta = \frac{2\alpha}{\pi x}\cdot(2ln\frac{\sqrt{s}}{m_e} - 1),$$

and δ takes into account vertex and self-energy corrections. At the $\Upsilon(4S)$ energy, $\beta = 0.088$ and $\delta = 0.067$.

For a hadronic final state, f, the normalized cross section at c.m. energy squared s', $\sigma_f(s')$, is obtained by relating the observed number of events in an interval ds' centered at s', $dN_{f\gamma}$, to the corresponding number of radiative dimuon events, $dN_{\mu\mu\gamma}$, by means of

$$\sigma_f(s') = \frac{dN_{f\gamma}\cdot\varepsilon_{\mu\mu}\cdot(1+\delta^{\mu\mu}_{\rm rad})}{dN_{\mu\mu\gamma}\cdot\varepsilon_f\cdot(1+\delta^{f}_{\rm rad})}\cdot\sigma_{e^+e^-\to\mu+\mu-}(s'),$$

where $s' = s(1-x)$; $\varepsilon_{\mu\mu}$ and ε_f are detection efficiencies, and $1+\delta^{\mu\mu}_{\rm rad}$, $1+\delta^{f}_{\rm rad}$ are final state radiative correction factors. The radiative corrections to the initial state, acceptance for the ISR photon, and virtual photon properties are the same for $\mu^+\mu^-$ and f, and cancel in the ratio.

2. $\mu^+\mu^-\gamma$ FINAL STATE AND EFFECTIVE LUMINOSITY

BABAR provides excellent particle identification (PID) information, and this permits the selection of two-prong events containing a hard photon, for which at least one of the charged tracks is well-identified as a muon.

Figure 1 shows the $\mu^+\mu^-$ invariant mass distributions for these events when at least one track is muon-identified (upper histogram), and when both tracks are muon-identified (lower histogram). In the upper distribution, the peak at 0.8 GeV is due to $e^+e^- \to \rho\gamma \to \pi^+\pi^-\gamma$; it disappears almost entirely when the second track also is identified as a muon. A sharp peak due to J/ψ decay to $\mu^+\mu^-$ is present in both distributions.

Figure 2 is a close-up view of Figure 1 in the J/ψ region. A fit using a Gaussian line-shape and linear background gives ~ 2000 events from J/ψ decay, and there is a small signal due to $\psi(2S)$ decay at ~ 3.7 GeV.

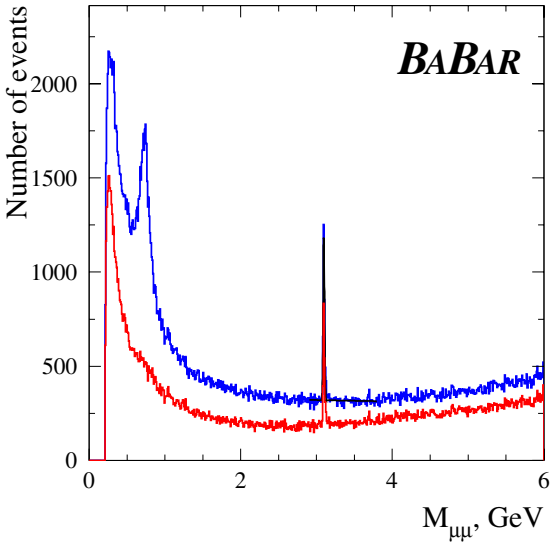

Figure 1: The $\mu^+\mu^-$ invariant mass distribution for two-prong events with a hard photon, when one track is identified as a muon (upper histogram), and when both tracks are muon-identified (lower histogram).

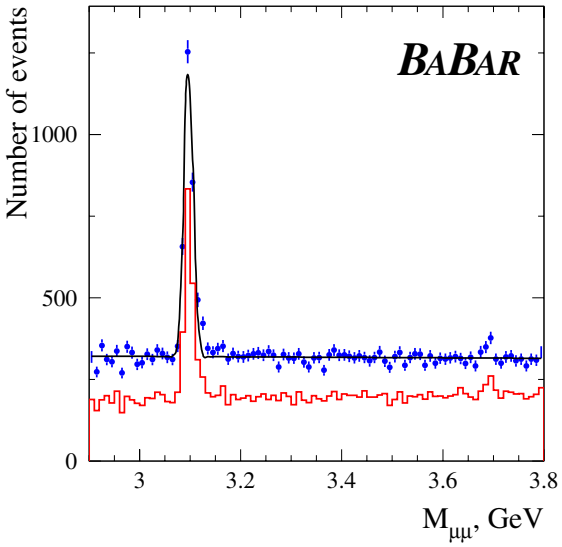

Figure 2: Figure 1 in the J/ψ region.

The $\mu^+\mu^-\gamma$ events can be used to normalize ISR production of hadronic final states. The invariant mass of the muon pair defines the effective collision energy, that is, the c.m. energy of the virtual photon. The energy dependence of the integrated luminosity, dL, for the interval dE_{γ^*} centered at virtual photon energy E_{γ^*} is then obtained from

$$dL(E_{\gamma^*}) = \frac{dN_{\mu\mu\gamma}(E_{\gamma^*})}{\varepsilon_{\mu\mu}\cdot(1+\delta^{\mu\mu}_{\rm rad})\cdot\sigma_{e^+e^-\to\mu^+\mu^-}(E_{\gamma^*})},$$

$$E_{\gamma^*} = m^{\mu\mu}_{\rm inv}$$

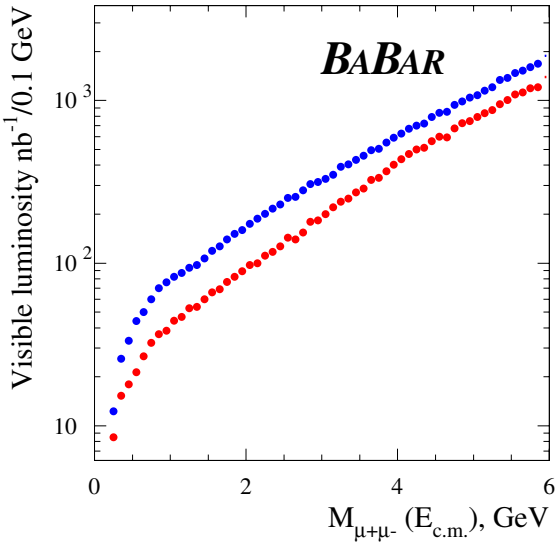

Figure 3: The visible (detected) integrated luminosity per 0.1 GeV for ISR at BABAR with no correction for acceptance and final state radiation when at least one track is muon-identified (upper distribution), and when both tracks are muon-identified (lower distribution).

where $dN_{\mu\mu\gamma}$ is the number of dimuon events observed in this interval. Figure 3 shows the energy dependence of the visible (that is, not corrected for acceptance and final state radiation) luminosity integrated over 0.1 GeV intervals. The upper distribution is obtained when at least one final state track is identified as a muon, while the lower requires both tracks to be muon-identified.

An advantage deriving from the use of ISR is that the entire range of effective collision energy is scanned in one experiment. This avoids the relative normalization uncertainties which can arise when data from different experiments are combined. The present BABAR data are equivalent to an e^+e^- machine scan in 0.1 GeV steps with a luminosity integral per point varying from $\sim 100\,{\rm nb}^{-1}$ at 1 GeV to $\sim 1\,{\rm pb}^{-1}$ at 5 GeV c.m. energy. A disadvantage is that invariant mass resolution limits the width of the narrowest structure which can be measured via ISR production. The resolution can be monitored directly using the width of the J/ψ signal; by using a kinematic fit, a value of ~ 8 MeV can be achieved for $\mu^+\mu^-$ events.

3. TWO HADRON FINAL STATES

3.1. $\pi^+\pi^-\gamma$ selection

The general selection criteria are the same for $\pi^+\pi^-\gamma$ and for $\mu^+\mu^-\gamma$ events. However, $\pi^+\pi^-$ selection requires that neither final state charged track be identified as a muon, kaon or proton (charge conjugation is implied throughout this paper, whenever relevant). The ρ peak dominates the resulting dipion invariant mass distribution, but for mass greater than

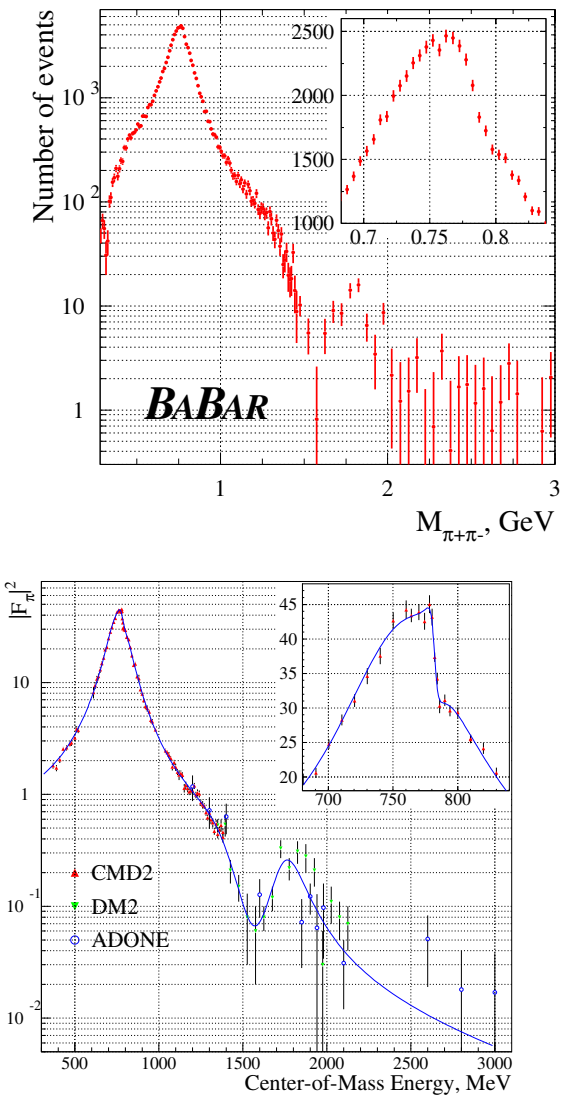

Figure 4: The uncorrected $\pi^+\pi^-$ invariant mass distribution for $\pi^+\pi^-\gamma$ events from BABAR (top), compared to pion form factor measurements from VEPP-2M and DCI (bottom).

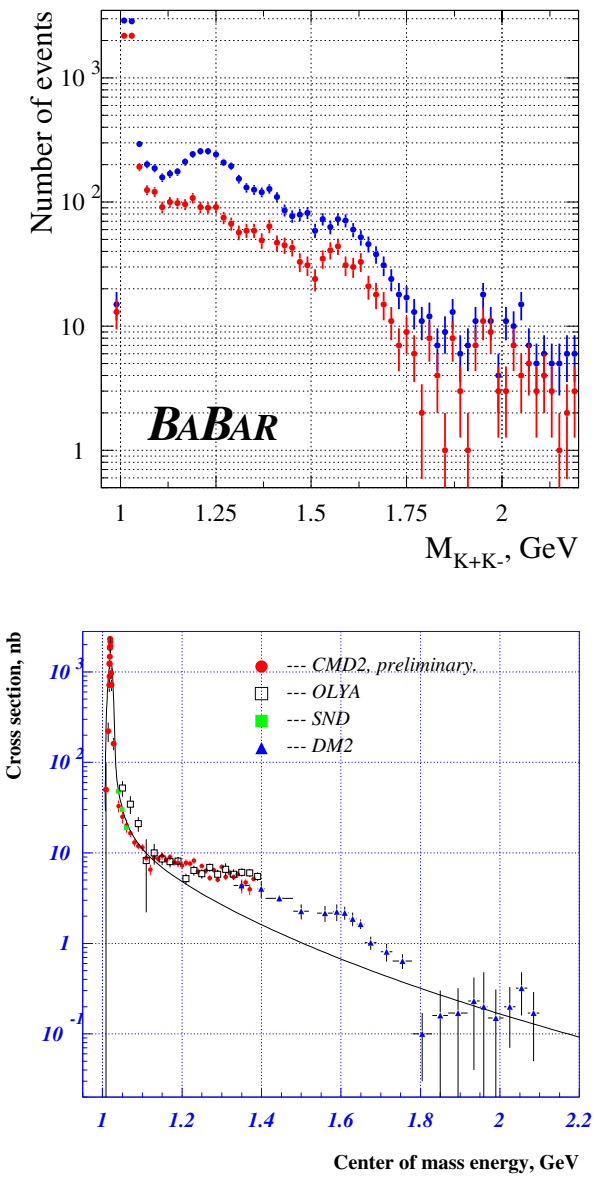

Figure 5: The uncorrected K^+K^- invariant mass distribution for $K^+K^-\gamma$ events from BABAR (top), compared to K^+K^- cross section measurements from VEPP-2M and DCI (bottom).

2.0–2.5 GeV, dimuon feedthrough is the main contribution to the spectrum.

Assuming the dipion contribution above 3.5 GeV to be negligible compared to that from dimuon background, the mass distribution of Figure 1 can be normalized to this region and used in a background subtraction over the entire mass range.

The resulting distribution is compared in Figure 4 (top) to data on the pion form factor (bottom) [7]. The agreement is very encouraging. The insets show the $\rho - \omega$ interference region. The form factor data show clear evidence of e.m. mixing, and although there is evidence of similar behavior in the data from BABAR, it is less sharply defined as a consequence of the poorer mass resolution ($\sim$ 13 MeV at the ρ meson peak). Nevertheless, the effect appears to be present.

3.2. $K^+K^-\gamma$ selection

The requirement that at least one final state track be identified as a kaon, and that neither be identified as a muon, pion or proton, leads to a rather clean sample of $K^+K^-\gamma$ events. The resulting K^+K^- invariant mass distribution is shown in Figure 5 (top) in comparison to the corresponding cross section measurements from VEPP-2M and DCI (bottom). Both distributions show a clear ϕ peak. The upper BABAR data points are obtained by requiring that at least one kaon be identified, while the lower require that both be identified. The structure at $\sim$ 1.2 GeV in the upper distribution is due to feedthrough from the ρ; it is almost entirely suppressed in the lower distribution, in-

dicating the effectiveness of the kaon identification procedure. The lower spectrum agrees quite well with the cross section data (bottom), and it will be of interest to learn whether or not the peaks in the BABAR data at $\sim$ 1.6 GeV and $\sim$ 2.0 GeV, which are less clear in the cross section data, are real.

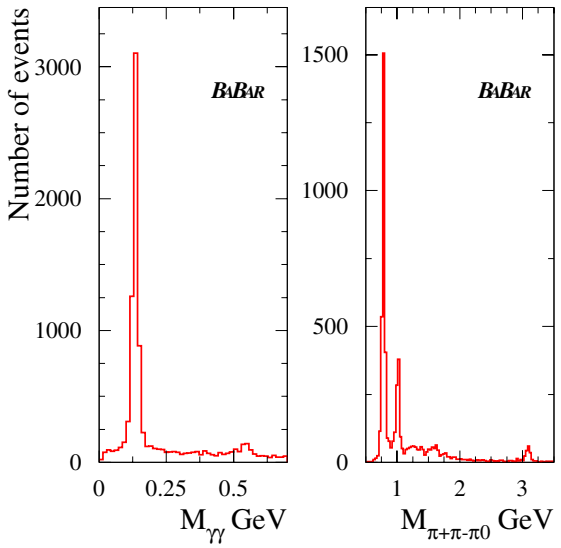

Figure 6: The $\gamma\gamma$ invariant mass distribution for $\pi^+\pi^-\gamma\gamma$ events (left); the combinations in the π^0 region were used to construct the three pion invariant mass distribution shown in the right-hand figure.

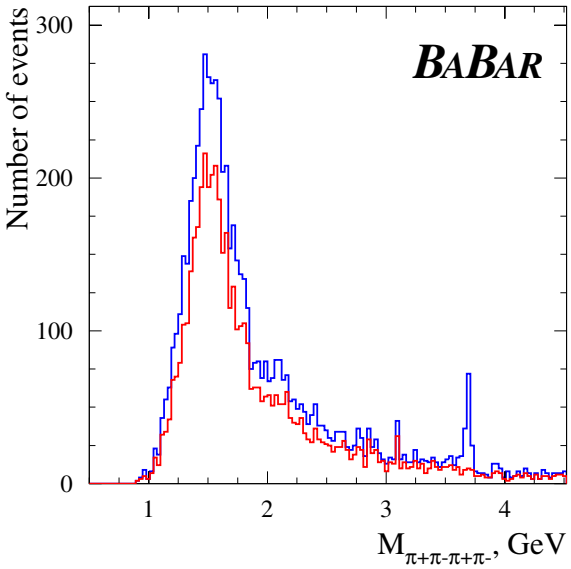

Figure 7: The invariant mass distribution for four-prong ISR events from BABAR when no track is identified as a kaon or proton (upper histogram), and when in addition no track is identified as a muon (lower histogram).

4. $\pi^+\pi^-\pi^0$ AND $\pi^+\pi^-\eta$ FINAL STATES

For events with several photons, the most energetic with energy greater than 1.0 GeV is interpreted as an ISR candidate. The remaining photons having energy greater than 100 MeV are then used in a π^0 and/or η search.

Two-prong events, with both tracks identified as pions, were required to have three photons in addition to the ISR candidate. The invariant mass distribution for the two softest photons from such events is shown in Figure 6 (left). Peaks are observed at the π^0 and η mass positions. Defining a π^0 candidate by $|m_{\gamma\gamma} - m_{\pi^0}| < 40$ MeV, the three pion invariant mass distribution is as shown in the right-hand plot. Clear peaks due to the ω, ϕ and J/ψ mesons are observed, indicating that data samples corresponding to the ISR production of these states with subsequent three-pion decay can be readily selected.

5. FOUR PION FINAL STATES

5.1. $\pi^+\pi^-\pi^+\pi^-$ final state

A relatively clean sample of four-pion candidate events is selected by requiring that, in addition to the ISR candidate photon, there be four charged tracks, none of which is identified as a kaon or proton. Figure 7 shows the mass distribution for the four charged tracks from such events (upper histogram). There is a narrow peak at the $\psi(2S)$ due to the decay $\psi(2S) \to \pi^+\pi^- J/\psi$ with $J/\psi \to \mu^+\mu^-$; this is removed by the additional requirement that no track be identified as a muon (lower histogram).

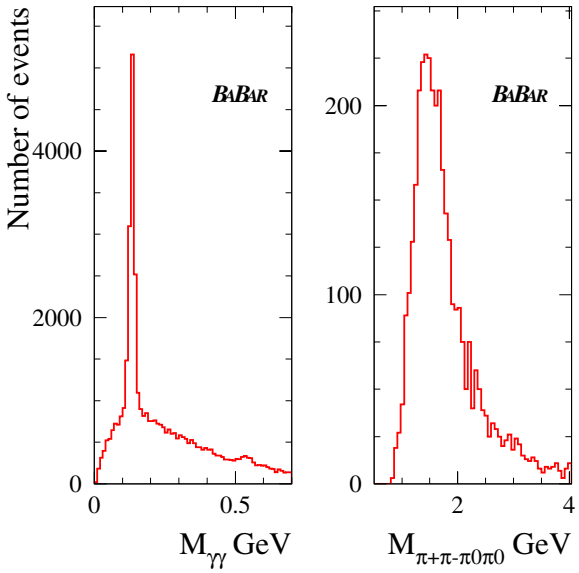

Figure 8: The two photon invariant mass distribution from $\pi^+\pi^-4\gamma$ ISR events (left) and the four pion invariant mass distribution obtained when two distinct photon combinations are in the π^0 mass region.

5.2. $\pi^+\pi^-\pi^0\pi^0$ final state

This final state is selected by requiring that two charged tracks and five photons be produced. The most energetic photon is assumed to be due to ISR, and the mass distribution for all possible pair combinations of the other four is shown in Figure 8 (left). Peaks due to π^0 and η production are seen. The requirement that two distinct combinations be in the π^0 mass range yields the four-pion mass distribution shown in the right-hand plot. It is very similar to that obtained for four charged pions.

The BABAR data can be compared to existing e^+e^- cross section measurements for four-pion final states. Figure 9 compares four-charged-pion cross section measurements from e^+e^- colliders (top) to the corresponding BABAR ISR data. A similar comparison is made in Figure 10 for $\pi^+\pi^-\pi^0\pi^0$ data. In general, the ISR data and the cross section data seem to agree in shape, but it is clear that the former suffer much less from the relative normalization uncertainties present in the latter.

5.3. Combined Analysis

For a multi-pion final state, it is important to understand the mass structure present in the contributing multi-pion subsystems, both from the standpoint of spectroscopy, and for the understanding of acceptance effects. In this regard, it is very useful to have information available for different isotopic spin configurations. This has been demonstrated in a four-pion analysis performed by the CMD-2 group [9], which was recently confirmed by CLEO using τ decays [10]. Both analyses demonstrate $a_1(1260)\pi$ dominance in four-pion production.

Further confirmation, and in fact more detailed study (because the phase space is not limited), can be obtained from ISR production of four-pion final states. For example, Figure 11 shows the three-pion mass distributions resulting from the ISR production of $\pi^+\pi^-\pi^+\pi^-$ and $\pi^+\pi^-\pi^0\pi^0$ events in the BABAR data. It is clear that an intermediate $\omega\pi^0$ state contributes to $\pi^+\pi^-\pi^0\pi^0$, and that both final states exhibit a broad peak which may be due to the $a_1(1260)$ resonance.

6. HIGHER MULTIPLICITY FINAL STATES

The good resolution and PID characteristics of the BABAR detector permit ready selection and study of even higher multiplicity final states produced exclusively (that is, with no undetected final state particles) via ISR. For example, data samples for the hadronic states $K^+K^-\pi^+\pi^-$, $2(\pi^+\pi^-)\pi^0$, $6\pi(charged)$, $2(\pi^+\pi^-\pi^0)$ and $3(\pi^+\pi^-)\pi^0$ have been selected, and already contain a few thousand events each. Normalization to $\mu^+\mu^-\gamma$ will enable cross section measurements for these processes in the 1–5 GeV c.m. energy range. These final states have not been studied at e^+e^- colliders, and so new information on meson spectroscopy etc. is already contained in the present BABAR data sample, with the prospect of a factor of ten increase in statistics over the next few years.

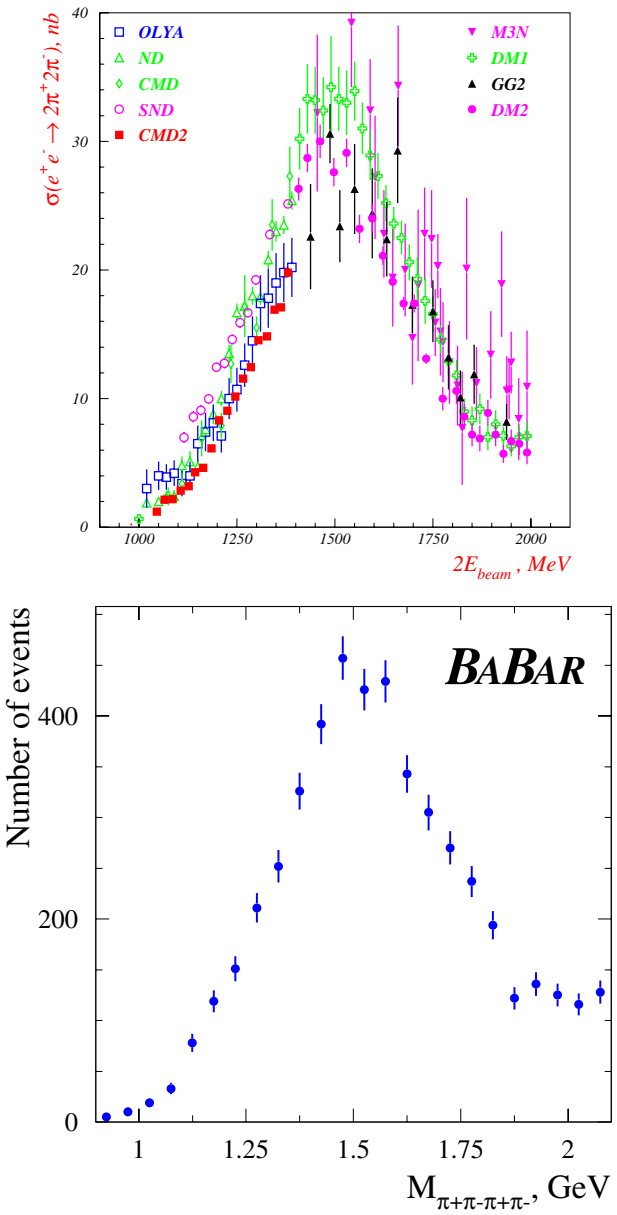

Figure 9: The c.m. energy dependence of the $\pi^+\pi^-\pi^+\pi^-$ cross section measured in e^+e^- experiments (top) compared to the corresponding uncorrected mass distribution from BABAR ISR data (bottom).

7. SUMMARY

- The good resolution and PID capabilities of the BABAR detector permit the identification and measurement of a broad range of final states produced at low effective c.m. energy via ISR during data-taking in the $\Upsilon(4S)$ energy region.
- Specifically, the observation of low mass 1^{--} resonances has been demonstrated, and it appears that a great deal of additional information about meson spectroscopy can be extracted from the data.

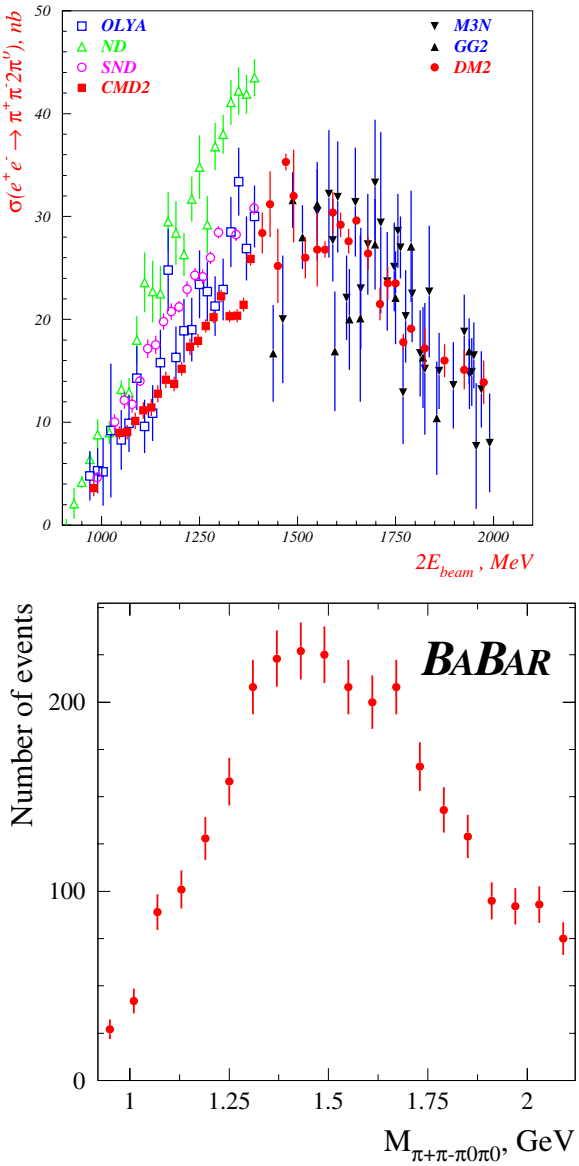

Figure 10: The c.m. energy dependence of the $\pi^+\pi^-\pi^0\pi^0$ cross section measured in e^+e^- experiments (top) compared to the corresponding uncorrected mass distribution from BABAR ISR data (bottom).

- The present BABAR data in the 1.4–3.0 GeV mass range are already comparable in quality and precision to direct measurements from the DCI and ADONE machines, and do not suffer from the relative normalization uncertainties which seem to exist for certain final states.
- If luminosity and efficiency can be understood with 2–3% accuracy, ISR production with the BABAR detector should yield useful measurements of R, the ratio of the hadronic and dimuon cross section values, in the low-energy regime of e^+e^- collisions.

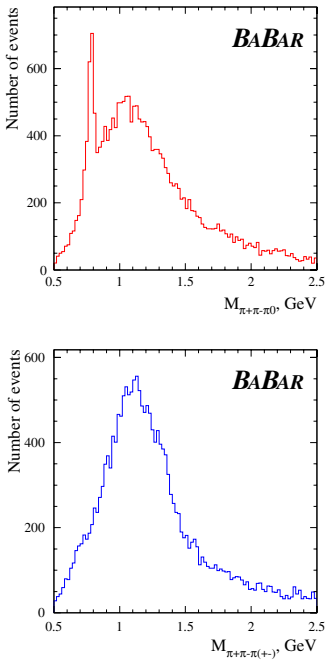

Figure 11: Three pion mass distributions for the $\pi^+\pi^-\pi^0\pi^0$ and $\pi^+\pi^-\pi^+\pi^-$ final states produced via ISR.

REFERENCES

[1] M. Benayoun, S.I. Eidelman, V.N. Ivanchenko, Z.K. Silagadze, "Spectroscopy at B-factories Using Hard Photon Emission," Modern Phys.Lett. A. Vol.14, No.37(1999)2605.

[2] S. Binner et al., Phys. Lett B **459**(1999)279; J.Kuehn, hep-ph/0101100.

[3] Vuko Brigljevic (LLNL), "Study of $e^+e^- \to \phi\gamma$ events," BABAR internal documentation, July 14, 2000.

[4] X.C. Lou (UT Dallas), W. Dunwoodie (SLAC), "Production of the $\psi(2S)$ via Initial State Radiation at the $\Upsilon(4S)$ Energy," BABAR internal documentation, Aug. 12, 2000.

[5] D.E. Groom et al., Eur. Phys. J. C **15** (2000)1.

[6] F.Fabozzi et al., "Muon Identification in the BaBar Experiment," BABAR internal documentation, June 21, 2000.

[7] R.R. Akhmetshin et al., "Measurement of pion form factor around ρ resonance with CMD-2 detector," BINP Preprint 99-10, Novosibirsk, 1999.

[8] M.N. Achasov et al. (SND Collaboration), Phys. Lett. B **462**(1999)365.

[9] R.R. Akhmetshin et al. (CMD-2 Collaboration), Phys. Lett. B **466**(1999)392.

[10] A.J. Weinstein et al.(CLEO Collaboration), "Semi-hadronic τ decays at CLEO," Nucl. Phys. Proc. Suppl. **98**(2001)261.

[11] R.R. Akhmetshin et al. (CMD-2 Collaboration), Phys. Lett. B **489**(2000)125.